Effect of cohesion and shear modulus on the stability of a stretched granular layer

Hector Alarcon, Jean-Christophe Géminard, Francisco Melo

▶ **To cite this version:**

Hector Alarcon, Jean-Christophe Géminard, Francisco Melo. Effect of cohesion and shear modulus on the stability of a stretched granular layer. Physical Review E : Statistical, Nonlinear, and Soft Matter Physics, 2012, 86, pp.061303. hal-00763714

HAL Id: hal-00763714
https://hal.science/hal-00763714

Submitted on 11 Dec 2012

HAL is a multi-disciplinary open access archive for the deposit and dissemination of scientific research documents, whether they are published or not. The documents may come from teaching and research institutions in France or abroad, or from public or private research centers.

L'archive ouverte pluridisciplinaire **HAL**, est destinée au dépôt et à la diffusion de documents scientifiques de niveau recherche, publiés ou non, émanant des établissements d'enseignement et de recherche français ou étrangers, des laboratoires publics ou privés.

The effect of cohesion and shear modulus on the stability of a stretched granular layer.

Hector Alarcón, Jean-Christophe Géminard † and Francisco Melo.
Departamento de Física, Universidad de Santiago de Chile,
Av. Ecuador 3493, Casilla 307, Correo 2, Santiago, Chile. and
† *Université de Lyon, Laboratoire de Physique, Ecole Normale Supérieure de Lyon,*
CNRS, UMR 5672, Laboratoire, ENS, Université, 46 Allée d'Italie, 69007 Lyon, France.

The main mechanism of the cellular pattern which forms at the surface of a thin layer of a cohesive granular material submitted to in-plane stretching has been identified as the "strain softening" arising from the features of grain-grain interactions. We perform novel measurements of the strain field associated with such structures by using a correlation image technique and additionally characterize the cohesion and shear modulus of the samples. We show that for high cohesion the layer is fragile and the surface deformation is highly non linear, whereas at low cohesion, a smooth and linearly growing structure is observed as a function of external stretching. Analysis of the wavelength as a function of cohesion along with independent measurement of the shear modulus indicate that a simple model of strain-softening is acceptable if a mechanism of cluster formation due to cohesion is taking place.
PACS: 89.75.Kd: Pattern formation in complex systems; 83.60.Uv: Rheology: fracture; 45.70.Qj: Pattern formation in granular matter

I. INTRODUCTION

Wet granular materials are characterized by a network of liquid bonds inducing attractive capillary forces between particles [1, 2]. Depending on the liquid content several regimes are identified leading to different scalings for the cohesion force [2, 3]. A relevant feature, nearly independent of the liquid content, is the "strain softening" due both to a decrease of the associated adhesion force when a single bridge elongates [4] and to a decrease in the overall number of bridges which collapse when excessively stretched [5]. This effect can be seen as responsible for the relatively low plasticity of cohesive granular materials under tension and provides some clues why structures made of humid sand, such as sandcastles, generally break in a catastrophic manner. In practice the softening behavior is observed above a critical strain which is associated with the initial compression of the grains induced by the suction force due to the capillary bridges [6].

In a recent article [7] we explored the response of a horizontal thin layer of cohesive material to the simplest mode of deformation. An extensible membrane provided a suitable system to introduce an overall homogeneous deformation on the layer. It was shown that "strain softening" was responsible of the nearly periodic structure that develops, modulating the strain field in the layer along the pulling axis, as soon as the external deformation was turned on. The measured wavelength of the structure resulted linearly dependent on the layer thickness, almost independent on particle size and a linear function of the relative humidity. The fracturing of a cohesive granular layer subjected to flexural deformation, investigated recently [8], has shown similar features.

In the present manuscript, we explore further the "strain softening" as a mechanism of mechanical instability in a cohesive layer. We present novel measurements, obtained from an image-correlation technique, of the strain field associated with the cellular instability and characterize the cohesion and the shear modulus of the samples.

Image correlation analysis makes possible to show that two distinct regimes of layer response appear as a function of the cohesion. For high cohesion the surface deformation is highly non linear whereas at low cohesion a smooth and linearly growing structure is observed as a function of the external stretching. Aiming at establishing a more fundamental connection between the layer structure and the properties of the granular material, we develop experimental methods for the assessment of the cohesion and shear modulus as function of the particles diameter and of the relative humidity.

The analysis reported in Ref. [7] indicated that the wavelength, λ, increases with the relative humidity, and thus with the cohesion, for a given grains size but, surprisingly, that λ is nearly independent of the particle diameter at a given relative humidity, even if smaller grains are more cohesive in the sense that they exhibit larger angle of avalanche.

In Ref. [7] the results were reported in terms of the relative humidity or angle of avalanche as the mechanical properties of the material, especially the cohesion, were not measured. In the present manuscript, the cohesion and the shear modulus are directly measured and the instability is analyzed in terms of the latter mechanical characteristics of the granular material. Our measurements indicate that the simple model of strain-softening proposed in Ref. [7] is acceptable if a mechanism of cluster formation due to cohesion is at play.

II. EXPERIMENTAL SETUP AND PROTOCOLS

The experiment consists in imposing an in-plane deformation at the base of a thin layer of a cohesive granular material. To do so, the grains are initially spread onto

an elastic membrane to which the deformation is imposed (Fig. 1). The experimental set up used here has some improvement with respect to that described in Ref. [7]. A cross is cut from a thin latex membrane (thickness 0.5 mm, width 40 cm) and is maintained at its four ends by four horizontally movable jaws. In the central part of the set up, the membrane leans on a steady, horizontal, square table (width 10 cm). By displacing the jaws, whose movement can be prescribed independently by four computer controlled motors (Thorlabs Z825BV), a wide variety of planar deformations can be achieved. For the experiments described here, the jaws are controlled such that the membrane, which remains in the same horizontal plane above the table, extends along one axis but does not narrow in the perpendicular direction. We checked, using a correlation image technique described below, that the resulting overall strain field is homogeneous in the test region. As a result, the granular pattern is aligned perpendicularly to the pulling direction.

The granular material consists of spherical glass-beads (USF Matrasur, sodosilicate glass). We shall report results obtained for various samples in a large range of bead diameters d (0-45, 53-75, 106-125, 150-200 μm). Prior to each mechanical test, grains where cleaned to remove organic material and moisture. The mechanical properties of the granular matter put in contact with a humid atmosphere are likely to change with time (ageing) [9, 10]. In order to insure that they reached a nearly stationary state, the samples were kept in contact with the desired humidity environment for 1 hour previous to the experiments.

The mechanical properties of the cohesive granular material are assessed independently in two additional experiments. The cohesion is characterized by the tensile stress, σ_s, the force per unit surface one must apply to separate the material in two parts. In Ref. [7], the cohesion was indirectly accounted for by measurements of the avalanche angle, θ_a. However, the functional relation between σ_s and θ_a is complex and requires a previous calibration [9]. Aiming at measuring cohesion directly, we designed an experimental configuration to assess the pulling force arising when a suitable indenter is pulled apart from the surface of the granular sample. In section III A, the cohesion is obtained as the ratio of the maximum pulling force to the indenter section. In the theoretical approach, the second important parameter to compare the weakening to is the shear modulus. We report in section III B direct measurements of the shear modulus G as a function of cohesion in a range of normal stress which compares with the experimental conditions encountered in the tensile experiment.

In the tensile experiments, the sample is prepared first by pouring dry cleaned grains onto the membrane. The surface of the material is then leveled by means of a cylindrical rod guided by lateral spacers, which achieves a well-defined thickness h (from 1 to 10 mm, to within 0.1 mm). In order to tune the cohesion, the whole experimental device is placed in a chamber at constant humidity. The atmosphere is equilibrated with saturated salt solutions and relative humidity is monitored by means of a humidity meter (Lutron HT-3015). Unless specified, samples are aged during one hour at constant humidity prior to imposing the deformation.

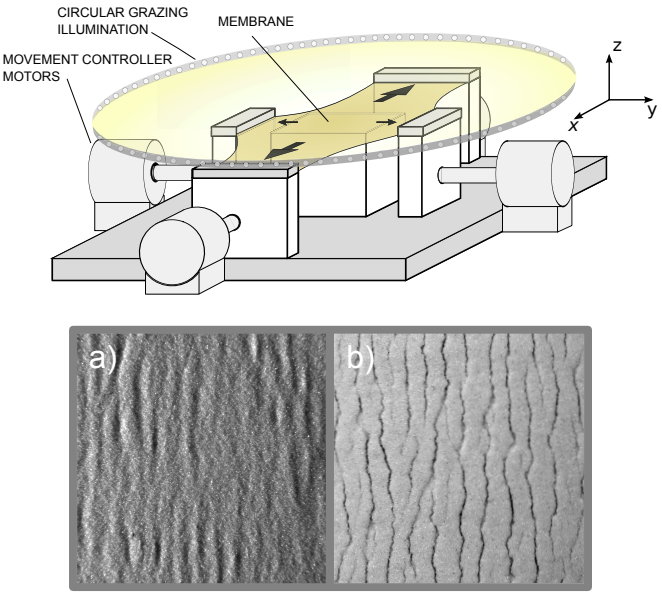

FIG. 1. (Color online) **Sketch of the experimental setup** – Each of the four arms of the cross-shaped membrane is independently driven by a computer-controlled motor so that a wide range of deformation modes can be achieved. For the reported experiments, uniaxial strain is achieved to better than 1% over a surface area of 50 cm^2. Lower panels: Typical cellular structures for two distinct values of the cohesion. (a) Low cohesion: $\sigma_s = 1$ Pa. (b) High cohesion: $\sigma_s = 4.1$ Pa [$h = 3$ mm, $d = 53 - 75$ μm and overall imposed stretching $\theta = 0.15$].

The free surface of the sample is imaged from above by means of a digital camera (Nikon DMX1200). A ring light-source (home-made arrays of LEDs, Fig. 1) located around the elastic band, a few centimeters above the table plane, provides a good contrast. Quantitative information is obtained by extracting the flow fields using an image cross-correlation technique. In order to assess non uniform flow fields (we shall see that a cellular instability indeed develops), we define a sliding window that scans the whole image and measure the local flow. The method gives a direct measure of the displacement field if interpreted as the average displacement of the cluster of beads enclosed by one subimage corresponding to the actual position of the sliding window. The size of the sliding window was approximately 1 mm^2 (containing about 100 particles) and moved at regular horizontal and vertical increments of 0.25 mm. The spacial resolution of the method is better than 1 mm and the strain sensitivity is of about 1 $m$strain.

III. RESULTS

A. Cohesion Assessment

To characterize the cohesion, we measure the force needed to pull a flat indenter apart from the free surface of the granular sample, as depicted Fig. 2. The indentor surface is coated with a layer of grains identical to the ones of the granular sample to be analyzed.

The indenter is first gently located in contact with the sample surface and the contact force (pushing force) is monitored by a sensitive enough analytical balance (Scaltec $SBA33$, 100 μg resolution). The initial pushing force is fixed at the same constant value for all samples. A computer controlled rotation stage (Thorlabs CR1/MZ6) ensures smooth approach and retraction of the indenter from the sample. As a check of repeatability, we report in Fig. 2b several behavior of the retraction forces as a function of the upward displacement of the indenter performed under nearly equal conditions. All curves present common features when the indenter is pulled back; first the weight on the balance quickly decreases, reaches a minimum and smoothly increases to reach a plateau. The force plateau is reached when capillary bridges are broken and the indenter no longer in contact with the sample. Thus, we identify the force difference between the minimum force and the plateau as the maximum pulling force, F_s, and the typical displacement, δ for the contact loss as a measure of a critical deformation for the rupture of the material (Notice that, given the small values of cohesive forces and the stiffness of the scale, the displacement of the sensitive part of the balance can be neglected with respect to that of the indenter). We consider that F_s relates with the tensile stress σ_s according to $F_s = \sigma_s S$ where S is the surface area of the contact between the indenter and the granular layer. Different surface area were tested. The results reported in Fig. 2c corroborate the linear dependence of F_s on S and, thus, validate the measurements of σ_s.

We report in Fig. 3 the tensile stress σ_s as a function of the particle size d, for various relative humidities R_H. Each point in the graph corresponds to the average of seven retraction trials. The dispersion in σ_s is of about 5%, the largest for the smallest R_H. The tensile stress σ_s decreases quickly when the particle size is increased, the decrease being faster for the larger humidity.

The rupture distance δ (Fig. 4) is also extracted from the retraction force curves by assuming an exponential dependence of the pulling force on the indentor displacement. Within the experimental errors, δ is almost independent of the particle size but is an increasing function of relative humidity. By plotting δ vs σ_s (since cohesion is a more natural variable in our experiment) for a given particle size, we observe that δ scales roughly as $\delta \approx d^2\sigma_s/\gamma_f$ where the experimental constant, which has the dimension of a surface energy, is $\gamma_f \approx 10$ mJ/m^2 (Fig. 4, inset).

We notice that in our experiments the water content is small even at relatively large humidity and that the measured tensile stress is small compared to that expected for a fully developed bridges regime ($\sigma_s \ll \pi\gamma/d$)[3] which suggests that particle roughness is playing an important role in the cohesion observed here. Thus, σ_s scales roughly as $1/d^2$ instead of $1/d$ as it would occur in the regime of fully developed capillary bridges. Formally, the

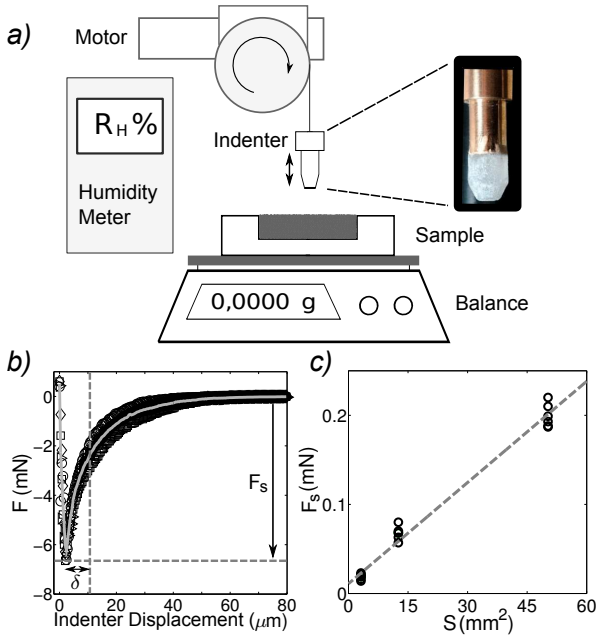

FIG. 2. **Cohesion assessment** – a) The force of cohesion F_s is measured by means of the analytical balance when the indentor is retracted at constant speed from the surface. The whole is inside a chamber at constant humidity. b) Several retraction curves: each curve showing a minimum (F_s) and a plateau after complete indenter retraction. Dashed line indicates the averaged force for indentor diameter $7.4mm$. c) Cohesion force, F_s, vs. indenter surface area,S.

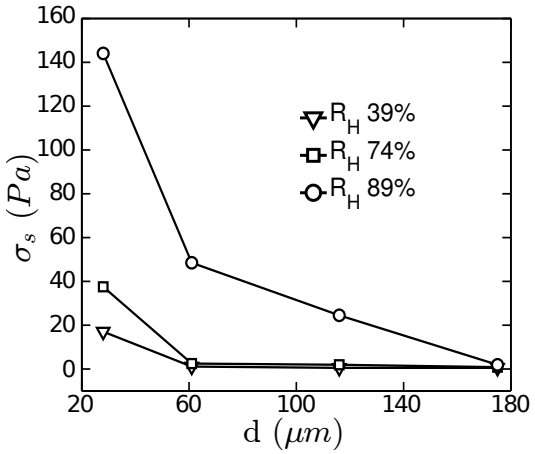

FIG. 3. **Tensile stress σ_s vs. grain size d for distinct relative humidity** R_H – [after 1 Hr of ageing].

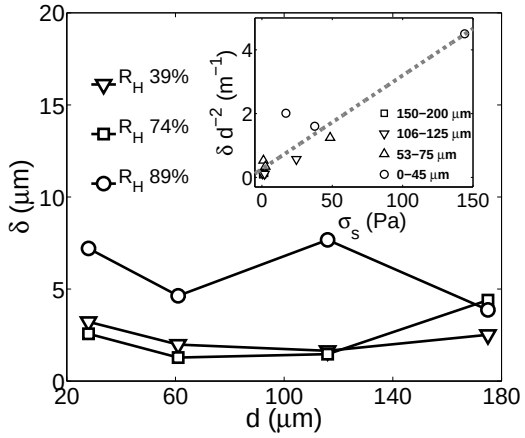

FIG. 4. **Rupture distance δ vs. particle size d for distinct values of R_H** – Inset: δ as function of σ_s for several values of d.

fully developed bridge regime should be obtained when δ tends to be of the order of d. Interestingly, δ is identified to be proportional to both the number of active sites, (for water nucleation), and their average radius of curvature. This identification is obtained by simple inspection of the expression for capillary force (See Eq. 6 in [11] for details) derived in the roughness regime presented in Refs. [9, 11].

In order to provide some additional clues for the understanding of the mechanical behavior of our samples, we assessed the typical roughness of particles through the analysis of atomic force images of the particles surfaces (Fig. 5). Scales of typical height l_R and typical width l_W of the roughness are extracted from the images by filtering the asperities, which were less than a few nanometers in typical size. Table I summarizes our findings which indicate that l_R and l_W do not systematically depend on the particle size, d.

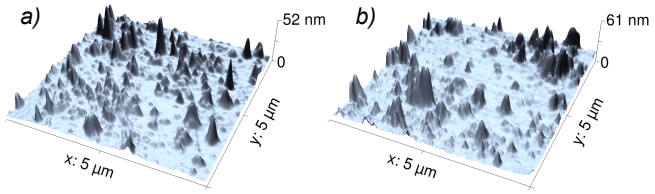

FIG. 5. (Color online) **AFM images of the particle surface** – a) Particle size, $d = 53$-75 μm b) $d = 106$-125 μm.

d (μm)	$0-45$	$53-75$	$105-125$	$150-200$
l_R (nm)	70	50	100	70
l_W (nm)	270	365	680	460

TABLE I. **Typical lengths l_R and l_W.**

For the purposes of the present study, we limit ourselves to the results presented above. A detailed analysis of the dependence of the cohesion on the experimental parameters such as the particles roughness, the particle size and the water content will be given elsewhere.

B. Shear modulus assessment

To characterize the shear modulus G, a Rheometer Anton Paar MCR-301 is used. It applies controlled shear stress and normal force to the sample (Fig. 6).

It is important to discuss the range of normal stress we use for this study. We are interested on the shear modulus at low confinement pressure. Indeed, given that the height of the layers is less than $h = 0.5$ cm, and that the layer density is of about 10^3 Kg/m^3, the maximum pressure at the layer base is less than 50 Pa, thus of the same order as the tensile stress due to moisture.

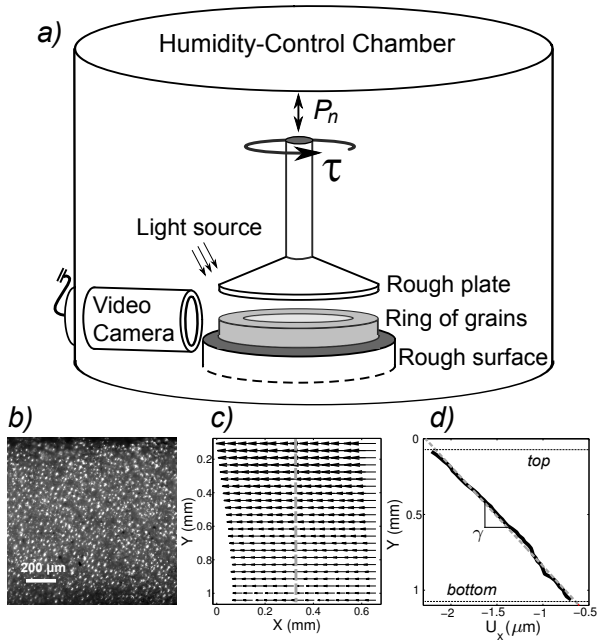

FIG. 6. **Shear modulus measurements** – a) Sketch of the setup. The sample is a ring of internal diameter 18 mm and of rectangular cross section of 4 mm in width by 1 mm in height. b) Image from the side of the granular sample. c) Displacement field, arrows indicating the grains displacement obtained by means of correlation analysis. d) Displacement profile. Horizontal lines indicate the top and bottom boundaries of the shear cell.

For the test, we build samples having the shape of a circular annulus with a rectangular cross section as illustrated in Fig. 6. Sand paper is glued to the upper and lower surfaces to avoid slippage. In order to insure reliable measurements, the applied shear stress and the resulting shear deformation in the whole sample thickness are measured independently. To do so, we analyze

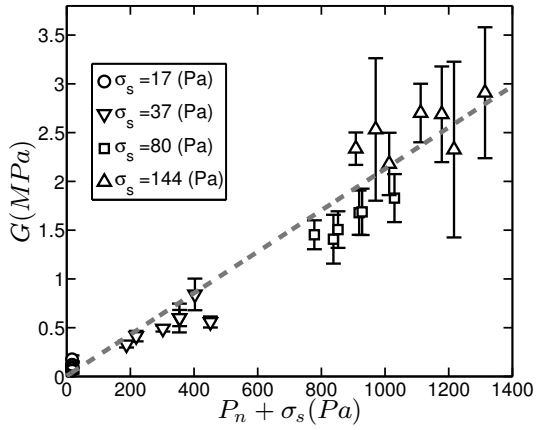

FIG. 7. **Shear modulus G vs. $\sigma_s + P_n$ for various cohesion** $-$ $[d = 0 - 45\mu\text{m}]$.

images of the layer taken from the side (Fig. 6). Image correlation analysis is used to obtain the shear field on a squared window of the sample. By plotting the shear stress against the shear strain, for given normal forces P_n, we obtained G for various humidity conditions.

Due to the necessity to build annular self-standing samples, only small particles which are cohesive enough are tested, $d = 30$ μm; small particles having highest cohesion allow us to scan a relatively wide range of R_H. In turn, larger particles, at low humidity, exhibit low cohesion which makes samples less stable when the normal force is increased. Measurements of the tensile stress are carried out in the same samples as soon as the shear test concludes to avoid ageing errors.

We report the shear modulus G as a function of the applied normal stress P_n for distinct values of the cohesion in Fig. 7. We notice that when G is plotted against $\sigma_s + P_n$ all results collapse in a single straight line, which indicates that the proper confinement pressure includes the additional contribution of the cohesion. This result is particularly interesting and deserves to be thoroughly discussed. For spheres interacting through a Hertz potential, G would scale has $P_n^{1/3}$. In turn, for a highly cohesive ensemble of Hertzian spheres it has been recently shown [13] that $G \sim E^{2/3}(\sigma_s + P_n)^{1/3}$, where E is the bulk modulus of the material. In our case, the linear dependence of G on P_n and the relative low values of the cohesion suggest that a different kind of elastic interaction is taking place. Let us consider that the contact between the spherical grains is dominated by rugosities or even asperities of typical size scale l_R. In this case, $F_s + N_n = JA_r$, where F_s and N_n are the capillary force and the applied normal force respectively, J is the yield stress of the material and A_r is the real area of contact. Consistently, for rugosity dominated contacts, the elastic force exhibits a linear dependence on the local strain, δ/l_R, so that $F_{el.} \approx EA_r\Delta\delta/l_R$. Considering that the shear modulus differs from the effective bulk modulus $E_{eff.} \propto (F_{el.}/d^2)/(\Delta\delta/d)$ only by a factor of the order of the unity [14] and including the geometric factor [13], we find,

$$G \approx \frac{Ed}{6Jl_R}(\sigma_s + P_n). \quad (1)$$

From experimental data, we obtain $E/(Jl_R) \approx 6\times10^8$ m. For $l_R \approx 100$ nm, a value that is obtained by measuring the spheres roughness from AFM images, the ratio E/J is estimated to be of about 40, which is an acceptable value given that a material deformed a few percents yields. Indeed, independent measurements for a sodosilicate glass provide typical values of $E \approx 70$ GPa and $J \approx 3$ GPa which gives a $E/J \approx 25$ [15]. In addition, in experiments of indentation on a plate of soda-lime-silica-glass, a current value is $E/J \approx 40$ [16]. On the other hand, as a check of consistency, it is interesting to ask for the fraction ψ, of contacts that are actually acting in the plastic regime with respect to the elastic ones, as given by the well known Greenwood-Williamson approach [17]. This is $\psi \equiv (l_R/\rho)^{1/2}E/J$, where ρ is the curvature radius of typical asperities, which is approximated to $\rho \approx l_W^2/8l_R$. With data in table I and taking $E/J \approx 40$, we find that $\psi \approx 20$ which is consistent with our hypothesis of plastified contacts.

C. Pattern characterization

When the membrane is stretched by imposing the homogeneous strain field of amplitude $\theta \equiv U_{xx}$ at the base of the granular layer, one observes, provided that the grains are small enough and/or the relative humidity, R_H, large enough, the growth of a rather regular pattern at the free surface (Fig. 1). Domains, made of stripes having a rather well-defined width and making an straight angle with the stretching direction (x-axis, Fig. 1), nucleate and grow.

The Fig. 8 presents the modulation of the displacement fields along the pulling direction (The imposed deformation is substracted from the measured displacement field). For the case of low cohesion, presented in the uppermost panels, even if the structure is barely visible from pictures, image correlation analysis reveals a small modulations whose amplitude increase with θ. We point out that as θ is increased, the pattern evolves toward a structure of a relatively well selected wavelength. Right panels on Fig. 8 include the displacement $U_x - \theta x$ and its respective strain $dU_x/dx - \theta$ along a selected line (dashed lines) parallel to the pulling direction. The strain varies smoothly.

By contrast, for relatively high cohesion, Fig. 8 (lowermost panels), a rather well-defined wavelength is observed, even at small stretching θ. Displacement and strain profiles indicate a nonlinear behavior since the early stages of the structure development. Large positive strains are localized whereas extended region poorly stretched are observed. As a consequence, when the

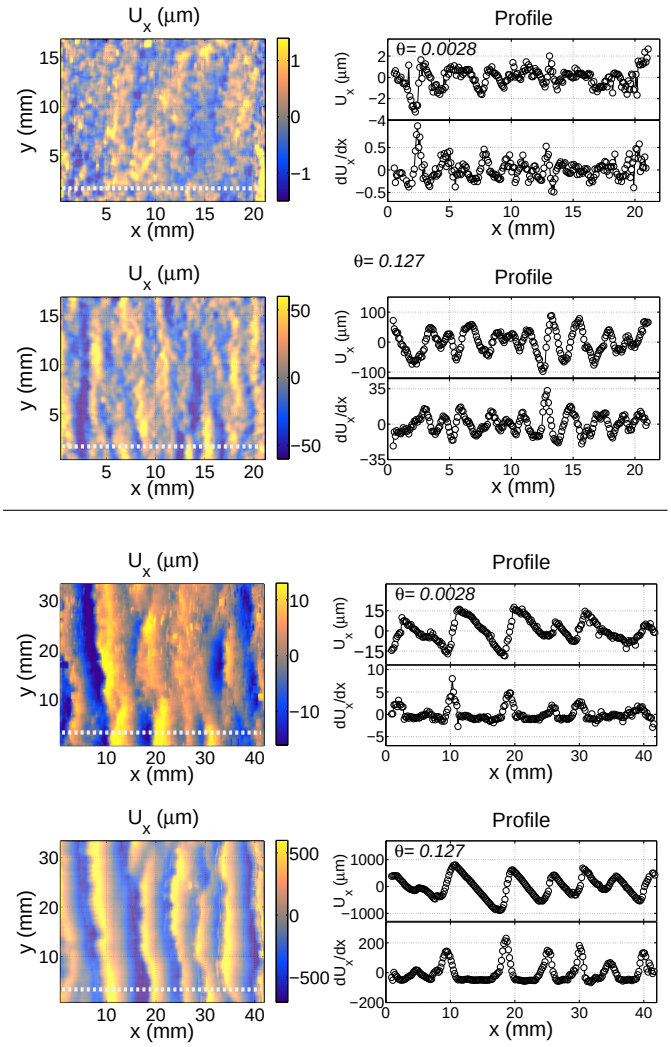

FIG. 8. (Color online) **Displacement fields for two distinct values of cohesion at a given thickness**– Left: Modulation of the displacement fields $U_x(x,y) - \theta x$. Right: Profiles of the modulation $U_x(x) - \theta x$ and associated modulation of the strain $dU_x/dx - \theta$ (in $m$strain) measured along the dashed lines. Results are reported for low cohesion, $\sigma_s = 1$ Pa (uppermost panel) and relatively high cohesion, $\sigma_s = 10$ Pa (lowermost panel) and for two values of the imposed stretching, $\theta = 0.0028$ and $\theta = 0.127$, as indicated on panels [$h = 5$ mm, $d = 53 - 75\mu$m].

stretching is further increased, the structure develops with a continuous increase of the strain in localized regions, which leads to the fracture of the granular layer in these regions of focused dilations.

From now on, it is particularly interesting to consider the dependence of the amplitude A of the displacement-field modulation at the free surface as a function of the average strain imposed at the base plane, θ. The sensitivity of the image correlation method makes it possible to accurately determine the RMS amplitude (normalized to the average wavelength), A/λ, as a function of θ

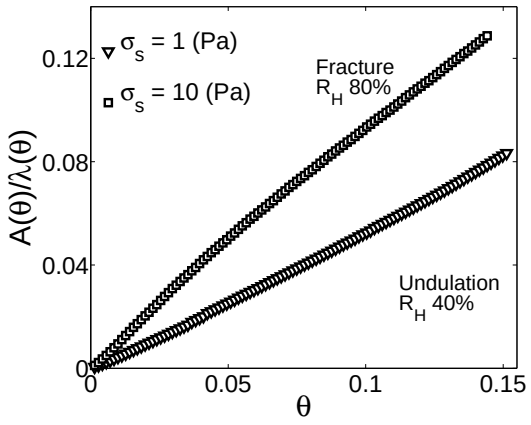

FIG. 9. **RMS amplitude of the strain variation along the stretching direction.** [Equal conditions as in Fig. 8].

(Fig. 9). One observes that the amplitude of the modulation starts growing linearly with θ, as soon as the layer is stretched. Confirming with a much better accuracy a result obtained in Ref. [7], these experiments prove that the instability does not exhibit any significant threshold in terms of deformation.

At this point, we consider the dependency of the typical wavelength, λ, of the fracture pattern on the cohesion. We first mention that λ is not strictly selected and that a large scatter on the stripes width is observed. In spite of the scatter, we observe that $\lambda \propto h$ in average. In Ref. [7], λ was observed to be almost independent of d for given relative humidity, R_H, and thickness, h. Here, our image analysis method allows the assessment of wavelength at very low cohesion for much lower imposed external displacement, which in turn minimizes scatter of the measurements. Fig. 10 presents the wavelength of the structure as function of relative humidity, R_H, as well as cohesion, accounted for by the tensile stress σ_s. For small R_H, λ is nearly independent on R_H but it strongly increases when R_H reaches a value about 70% (Note that such a relative humidity is typical of the transition between the roughness- and the smooth-sphere regimes for the capillary bridges [3]). However, when λ is plotted against σ_s only a slow increase is observed. Interestingly, when σ_s is used as independent variable instead of R_H, a small but significant dependence of λ on particle size, d, is revealed. In addition, at vanishing cohesion $\lambda \approx 0.6\ h$ independently of d.

IV. THEORETICAL ANALYSIS

In the following, we remind the main ideas presented in Ref. [7] on the mechanism of pattern formation on the cohesive layer. As observed in the section III A, due to the capillary nature of the interaction between the grains, the cohesion force decreases when the material is

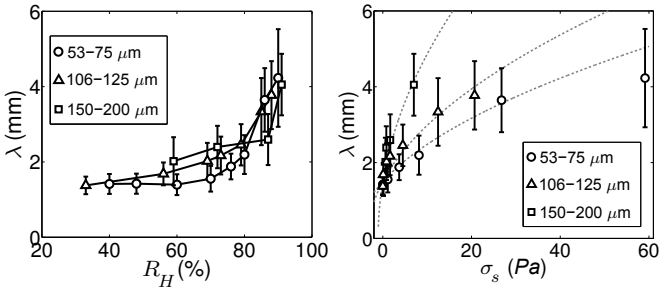

FIG. 10. **Left - Wavelength λ vs. relative humidity R_H. Right - Same vs. tensile stress** σ_s – Dashed lines are the best fit to λ obtained by using Eq. 6 with $\beta = (0.44 \pm 0.03)$ mJ/m^2. For $h = 3$ mm and $d = 53 - 75$ μm, $d = 106 - 125$ μm and $d = 150 - 200$ μm

.

stretched and, thus, grains are pulled apart [5, 6]. When the membrane is elongated, an homogeneous stretching of the material is imposed in the base plane. However, due to the "strain softening", in response to the overall stretch, the layer tends spontaneously to modulate the deformation. Indeed, regions of large deformation are associated with a smaller tensile modulus (cohesion) and regions of large modulus are associated with a smaller deformation, which results in an overall decrease of the energetic cost. Simultaneously, the modulation induces a shear deformation which is associated to an energetic cost. Thus, it is expected that the wavelength is governed by the balance of the gain associated with the modulation of the horizontal strain and of the loss associated with the resulting shear. In order to account for the experimental observations, let us first assume that the normal stress along the x-axis, σ_{xx}, decreases linearly with the uniaxial strain u_{xx}, according to $\sigma_{xx} = \sigma_s(1 - u_{xx}/\theta_m)$ when the material is stretched ($u_{xx} > 0$) [6]. The relation is no longer valid for $u_{xx} > \theta_m$, when the elongation is large enough for the bridges to collapse and, thus, the material to break apart. Thus, θ_m represents the typical strain for which a significant softening occurs whereas σ_s denotes the tensile stress previous to deformation. For the sake of simplicity, the contribution of the shear shall be accounted for by a simple shear modulus G whose value shall be discussed later. In this framework, the shear stress $\sigma_{xz} = G u_{xz}$ and, accordingly, the energy per unit volume

$$E = \sigma_s\Big(u_{xx} - \frac{u_{xx}^2}{2\theta_m}\Big) + \frac{1}{2}G u_{xz}^2. \qquad (2)$$

A sinusoidal perturbation of the displacement such that $u_x = \theta x + f(z)\sin(kx)$ in the horizontal plane is considered and, to obtain the associated displacement in the vertical direction u_z, dilation is neglected, $u_{xx} + u_{zz} = 0$. The wavelength $\lambda \equiv 2\pi/k$ is thus found to be proportional to h, independent of θ, according to $\lambda = 2\pi\frac{\sqrt{1+\xi}}{\arccos(-1/\xi)}h$, provided that $\xi \geq 1$, where $\xi \equiv 2\sigma_s/(G\theta_m)$. Thus, the layer is always unstable provided that the decrease in the tensile stress is large enough compared to the shear counterpart, i.e. $\frac{\sigma_s}{\theta_m} \geq \frac{G}{2}$.

The growth of the instability is limited by the condition that $u_{xx}(x,h) \geq 0$ for all x at the free surface and the amplitude of the vertical displacement, $k\,a$, is predicted to be proportional to $\theta\,h$.

V. DISCUSSION

Interestingly, the theoretical analysis, which involves both a decrease of the tensile stress associated with the stretching of the material and an energetic cost associated with the induced shear, predicts that a stretched layer is always unstable. In agreement with the experimental observations, the instability does not exhibit any finite threshold, the amplitude of the modulation increases linearly with θ (Fig. 9).

One important point is that the effect of the humidity content on the wavelength is accounted for by the dependence of λ on the ratio $\xi \equiv 2\sigma_s/(G\theta_m)$. For instance, in the limit of large ξ (small bridges), one expects

$$\lambda \simeq 4\sqrt{2\sigma_s/G\theta_m}h. \qquad (3)$$

As discussed in Ref. [7], the experimental increase of λ with R_H would impose, in the framework of the simplified model, that G increases slower than the ratio σ_s/θ_m. Note that σ_s and θ_m both should increase with R_H.

At the light of the measurements presented in section III B, the shear modulus G is indeed a linear function of σ_s. We obtained, $G \approx (\sigma_s + P_n)Ed/6Jl_R$, which replaced in Eq. 3, leads to

$$\lambda \simeq 4\sqrt{12\sigma_s J l_R/Ed\theta_m(\sigma_s + P_n)}h. \qquad (4)$$

Notice that, at the thicknesses explored in our experimental conditions, the pressure due to the grain weight at the base of the layer, $P_n \approx \rho g h$, is in most cases much smaller than σ_s, which allows us to neglect P_n for small h and sufficiently high σ_s. Thus, the dependence of λ on σ_s vanishes, indicating that the origin of the dependence of the wavelength on the humidity is not likely trough the variables discussed up to now. We notice that, the only remaining quantity which depends on R_H is θ_m. It is then natural to take θ_m as the typical strain necessary for rupture i.e., the ratio of the typical elongation for rupture δ_s to the typical size of the objet that is stretched L_c. Given the small water content in the system, it is reasonable to take δ_s as the typical size of the asperities, l_R. In addition, the water is likely to be heterogeneously distributed in the system and, thus, the grains to form wet clusters [2, 12]. To account for the clustering, we assume that $L_c \approx \alpha_s d/2$, where α_s is the typical size expressed in number of grains of a typical cluster in the system. With these assumptions, we get

$$\lambda \simeq 4\sqrt{6J\alpha_s/E}h, \qquad (5)$$

Finally, in order to account for the whole dependence of λ on the humidity, a guess for the dependence of the size of the clusters on the cohesion is necessary. Noticing that α_s must tend to one for vanishing σ_s and should be an increasing function of σ_s, we then write, $\alpha_s \approx 1+\sigma_s d^2/\beta l_R$, where β is a constant with the dimension of surface energy. The latter choice, which is motivated by the dependence of the elongation distance before rupture, δ, observed in the indentor experiment reported in section III A, correctly describes the functional dependence of λ on both σ_s and d. Indeed, the final expression

$$\lambda \simeq 4\sqrt{6J(1+\sigma_s d^2/\beta l_R)/E}h, \qquad (6)$$

predicts that, in the limit of small σ_s, independently of the choice for the scaling for clustering formation, $\lambda \approx 4\sqrt{6J/E}h$. Experimentally, we obtain $\lambda \approx 0.6h$, which predicts that $E/J \approx 200$ which is of the same order but significant larger than that obtained from shear modulus measurements (see section III B). Solids lines in Fig. 10 correspond to the best fit to λ using the values of l_R given in Table I and the constant β as unique free parameter. We get $\beta = (0.44 \pm 0.03)$ mJ/m^2. This value indicates that cluster size ranges from d to $10d$.

VI. CONCLUSIONS

In conclusion, we have presented novel measurements of the strain field associated to the instability of a stretched cohesive granular layer by image correlation analysis. The wavelength of the structure is an increasing function of both the cohesion and the particle diameter. The "strain softening mechanism" proposed in Ref. [7] along with novel measurements of tensile strength and shear modulus, lead us to hypothesize that a clustering effect might be at play.

ACKNOWLEDGMENTS

The authors acknowledge the financial support from the contracts ANR-CONICYT 011 (ANR-09-BLAN-0389-01) and anillo ACT95. The authors also would like to thank an anonymous reviewer for his contribution to the final discussion of our findings.

[1] Z. Fournier, *et. al.*, J. Phys.: Condens. Matter **17**, S477-S502 (2005).
[2] M. Scheel, R. Seemann, M. Brinkmann, M. Di Michiel, A. Sheppard, B. Breidenbach and S. Herminghaus, Nature **7**, 189-193 (2008).
[3] T. C. Halsey and A. J. Levine, Phys. Rev. Lett. **80**, 3141-3144 (1998).
[4] J. Crassous, E. Charlaix, and J.L. Loubet, Phys. Rev. Lett. **78**, 2425-2428 (1997).
[5] C. D. Willett, M. J. Adams, S. A. Johnson and J. P. K. Seville, Langmuir **16**, 9396-9405 (2000).
[6] T. Gröger, U. Tüzün and D. M. Heyes, Powder Tech. **133**, 203-215 (2003).
[7] H. Alarcón, O. Ramos, L. Vanel, F. Vittoz, F. Melo and J.-C. Géminard Phys. Rev. Lett. **105**, 208001 (2010).
[8] J.-C. Géminard, L. Champougny, P. Lidon and F. Melo, Phys. Rev. E. **85**, 012301 (2012).
[9] L. Bocquet, E. Charlaix, S. Ciliberto and J. Crassous, Nature **396** 735-737 (1998).
[10] S. Nowak, A. Samadani and A. Kudrolli, Nature Physics, **1**, 50-52 (2005).
[11] L. Bocquet, E. Charlaix and F. Restagno, C. R. Physique **3** 207215 (2002).
[12] M. Scheel, R. Seemann, M. Brinkmann, M. Di Michiel, A. Sheppard and S. Herminghaus, J. Phys.: Condens. Matter **20**, (2008) 494236.
[13] P.C.F Moller and D. Bonn EPL, **80**, 38002, (2007).
[14] L.D. Landau, E. M Lifchitz, *Theory of Elasticity* (Pergamon, New York, 1959).
[15] P. Forquin and F. Hild Adv. Appl. Mech., **44**, 1-72 (2010).
[16] J.T. Hagan, S. Van Der Zwaag J. Non-Cryst. Solids., **64**, 249268 (1984).
[17] See for instance, K. L. Johnson, *Contact Mechanics* (Cambridge University Press, Cambridge, 1985)